

# Glutamyl-prolyl-tRNA synthetase induces fibrotic extracellular matrix *via* both transcriptional and translational mechanisms

Dae-Geun Song,<sup>\*,†</sup> Doyeun Kim,<sup>‡</sup> Jae Woo Jung,<sup>§</sup> Seo Hee Nam,<sup>\*</sup> Ji Eon Kim,<sup>\*</sup> Hye-Jin Kim,<sup>\*</sup> Jong Hyun Kim,<sup>‡</sup> Seo-Jin Lee,<sup>¶</sup> Cheol-Ho Pan,<sup>†</sup> Sunghoon Kim,<sup>‡</sup> and Jung Weon Lee<sup>\*,‡,§,1</sup>

<sup>\*</sup>Department of Pharmacy, Research Institute of Pharmaceutical Sciences, College of Pharmacy, <sup>†</sup>Medicinal Bioconvergence Research Center, and <sup>§</sup>Interdisciplinary Program in Genetic Engineering, Seoul National University, Seoul, Republic of Korea; <sup>‡</sup>Systems Biotechnology Research Center, Korea Institute of Science and Technology (KIST), Gangneung-si, Republic of Korea; and <sup>¶</sup>Department of Life Science and Biotechnology, Shingyeong University, Gyeonggi-do, Republic of Korea

**ABSTRACT:** Fibrosis is characterized by the increased accumulation of extracellular matrix (ECM), which drives abnormal cell proliferation and progressive organ dysfunction in many inflammatory and metabolic diseases. Studies have shown that halofuginone, a racemic halogenated derivative, inhibits glutamyl-prolyl-transfer RNA-synthetase (EPRS)-mediated fibrosis. However, the mechanism by which this occurs is unclear. We explored the mechanistic aspects of how EPRS could develop liver fibrotic phenotypes in cells and animal models. Treatment with TGF- $\beta$ 1 up-regulated fibronectin and collagen I levels in LX2 hepatic stellate cells. This effect was inhibited in prolyl-transfer RNA synthetase (PRS)-suppressed LX2 cells. Using the promoter luciferase assay, TGF- $\beta$ 1-mediated collagen I,  $\alpha$ 1 chain transcription and  $\gamma$ 2 basal laminin transcription in LX2 cells were down-regulated by EPRS suppression, suggesting that EPRS may play roles in ECM production at transcriptional levels. Furthermore, signal transducer and activator of transcription (STAT) signaling activation was involved in the effects of TGF- $\beta$ 1 on ECM expression in a PRS-dependent manner. This was mediated *via* a protein-protein complex formation consisting of TGF- $\beta$ 1 receptor, EPRS, Janus kinases, and STAT6. Additionally, ECM expression in fibrotic livers overlapped with EPRS expression along fibrotic septa regions and was positively correlated with STAT6 activation in carbon tetrachloride-treated mice. This was less obvious in livers of *Eprs*<sup>-/+</sup> mice. These findings suggest that, during fibrosis development, EPRS plays roles in nontranslational processes of ECM expression *via* intracellular signaling regulation upon TGF- $\beta$ 1 stimulation.—Song, D.-G., Kim, D., Jung, J. W., Nam, S. H., Kim, J. E., Kim, H.-J., Kim, J. H., Lee, S.-J., Pan, C.-H., Kim, S., Lee, J. W. Glutamyl-prolyl-tRNA synthetase induces fibrotic extracellular matrix *via* both transcriptional and translational mechanisms. *FASEB J.* 33, 4341–4354 (2019). www.fasebj.org

**KEY WORDS:** fibrotic animal model • hepatic stellate cells • prolyl-tRNA-synthetase • signal transduction • STAT6

**ABBREVIATIONS:** 3D, 3-dimensional; *ACTA2*,  $\alpha$ -smooth muscle actin;  $\alpha$ -SMA,  $\alpha$ -smooth muscle actin; AAR, amino acid response; ALP, alkaline phosphatase; ALT, alanine transaminase; AST, aspartate transaminase; ATF, activating transcription factor; BDL, bile duct ligation; CCL<sub>4</sub>, carbon tetrachloride; Col1a1, collagen I  $\alpha$ 1; ECM, extracellular matrix; EPRS, glutamyl-prolyl-transfer RNA-synthetase; FN1, fibronectin; HCC, hepatocellular carcinoma; HF, halofuginone; HFF, human foreskin fibroblast; HSC, hepatic stellate cell; JAK, Janus kinase; KRS, lysyl-tRNA synthetase; LAMC2, laminin  $\gamma$ 2; MSC, multi-aminoacyl-tRNA synthetase complex; PRS, prolyl-tRNA synthetase; qRT-PCR, quantitative RT-PCR; sh, short hairpin; SMAD3, SMAD family member 3; STAT, signal transducer and activator of transcription; TGF- $\beta$ R1, TGF- $\beta$  receptor 1; tRNA, transfer RNA; WT, wild type

<sup>1</sup> Correspondence: College of Pharmacy, Seoul National University, 1, Gwanak-ro, Gwanak-gu, Seoul 08826, Republic of Korea. E-mail: jwl@snu.ac.kr

doi: 10.1096/fj.201801344RR

This article includes supplemental data. Please visit <http://www.fasebj.org> to obtain this information.

Liver fibrosis involves the excessive production and deposition of extracellular matrix (ECM) outside of cells after chronic injury-mediated inflammation (1). Chronic liver disease can progress to advanced fibrosis and cirrhosis, can accompany abnormal liver vascular architecture and functional failure, and can lead to hepatocellular carcinoma (HCC) (2). Significant advances in different cell and organism models have revealed molecular mechanisms that underlie the progression of liver fibrosis (3). Liver fibrosis involves a several-fold increase in the ECM (1). Liver ECM is produced mostly by hepatic stellate cells (HSCs) (4), and collagen I is the main component of the fibrous septa related to activated HSCs (5). Previous studies have shown that hepatocytes produce ECM *in vitro*. Furthermore, numerous other ECM molecules can be either indicators or therapeutic targets for manipulating fibrosis

(6), and the mammalian ECM consists of ~300 proteins (7). Because previous studies have mostly focused on the role of collagen I in liver malignancy, it is important to study the roles of other ECM molecules in liver fibrosis.

Pharmaceutical agents can be designed to prevent the progression of fibrosis and reverse steatohepatitis (8). Excessive ECM production by activated HSCs, portal myofibroblasts (MFs), and activated sinusoidal endothelial cells can be targeted in the development of antifibrotic agents (2). Moreover, ductular reactions or epithelial-mesenchymal transition-like changes can stimulate cholangiocytes, which then activate MF and result in the progression of cirrhosis and the development of HCC (9). Many different molecules are involved in signaling pathways for ECM production and deposition in these processes, leading to liver fibrosis. In particular, prolyl-transfer RNA (tRNA) synthetase (PRS) has been targeted to block fibrotic collagen production (10). Halofuginone (HF) is an analog of the alkaloid febrifugine that was originally isolated from the plant *Dichroa febrifuga*. HF is an excellent example of a bioactive agent that inhibits mRNA levels of collagen [collagen I  $\alpha 1$  (*COL1A1*) and collagen I  $\alpha 2$  (*COL1A2*)]. These levels are restored by proline supplementation (10), indicating that HF can block the catalytic activity of PRS, which involves the loading of proline to tRNA during the translational process of proline-rich collagen. The observation that both *COL1A1* (with 19% proline/total residues) and fibronectin (FN1) (with 7.9% proline/total residues) can be blocked by HF treatment (10) suggests that glutamyl-prolyl-tRNA synthetase (EPRS) may have roles beyond its translational tRNA charging activity. Limiting amino acids or inhibition of any of the aminoacyl-tRNA synthetases in animals activates the amino acid response (AAR) pathway after the accumulation of uncharged tRNAs is sensed and eukaryotic translation initiation factor 2 $\alpha$  is phosphorylated by GSN2 kinase (11). These processes lead to decreased global protein synthesis (12) and induction of selected genes, including activating transcription factor (ATF)4. ATF4 can then activate downstream genes to mediate the adaptation of cells to a stress environment, including C/EBP-homologous protein (CHOP, also known as DDIT3) (13). Thus, ATF4 protein expression activates multiple stress-induced genes, including AAR elements (14).

TGF- $\beta 1$  is a multifunctional cytokine that plays major roles in the initiation and progression of fibrogenesis and is the molecular basis of organ fibrosis (15). In fibroblasts from human patients, treatment with HF reduces TGF- $\beta 1$ -mediated collagen synthesis (16) without altering TGF- $\beta$  receptor gene expression or TGF- $\beta$  levels (17), indicating that HF targets downstream of TGF- $\beta$  receptor 1 (TGF- $\beta$ R1). HF can also target the signaling activity of SMAD family member 3 (SMAD3) and other molecules in different cell types (18). Furthermore, HF prevents the differentiation of Th17 cells, which are a subset of CD4<sup>+</sup> T cells that express IL-17. This occurs when HF binds to EPRS and induces the accumulation of uncharged tRNA and the activation of the AAR pathway and leads to the inhibition of autoimmune inflammation (19). Human glutamyl-tRNA synthetase and PRS activities are contained within a single polypeptide chain (20). Because of its

poor oral bioavailability, gastrointestinal toxicity, and limited patent life, the development of HF as an antifibrotic drug has been hindered (21). Many of its side effects may be due to its inhibition of TGF- $\beta$ /SMAD3 signaling, which is important for homeostatic immune and inflammatory functions (18,22). Thus, the role of EPRS in the development of fibrosis, especially regarding HF, requires further exploration.

In this study, we have focused on the mechanistic roles of EPRS in TGF- $\beta 1$ -mediated fibrosis. Our findings revealed relationships between EPRS and signal transducer and activator of transcription (STAT)6 during TGF- $\beta 1$ -mediated ECM production in LX2 HSCs and carbon tetrachloride (CCl<sub>4</sub>)-mediated liver fibrosis.

## MATERIALS AND METHODS

### Reagents and plasmids

All cytokines and growth factors, including TGF- $\beta 1$ , were purchased from Peprotech (Rocky Hill, NJ, USA). Halofuginone, CCl<sub>4</sub> (270652), ascorbic acid (A4403), poly(sodium 4-styrenesulfonate) solution (200 kDa, 30 wt. % in H<sub>2</sub>O; 561967), and the hydroxyproline assay kit (MAK008) were purchased from MilliporeSigma (Burlington, MA, USA). Bleomycin and target-specific pooled small interfering RNAs (siSTAT3 and siSTAT6) were purchased from Santa Cruz Biotechnology (Dallas, TX, USA). EPRS and its S999A mutant in pEXPR-103-Strep vector (IBA Lifesciences, Goettingen, Germany) were gifts from Dr. Myung Hee Kim (Korea Research Institute of Bioscience and Biotechnology). The PRS domain of EPRS was cloned into the pEXPR-103-Strep vector (IBA Lifesciences). Generation of pRc/CMV-WT STAT3 was performed as previously reported (23), and pCMV-STAT6-IRES-Neo was a gift from Axel Nohturfft (plasmid 35482; Addgene, Cambridge, MA, USA). Adenoviruses expressing SMAD2 or SMAD3 were explained in a previous study (24).

### Cell culture

LX2 HSCs were a kind gift from Dr. Scott Friedman (Ichan School of Medicine at Mount Sinai, New York, NY, USA), and human foreskin fibroblasts (HFFs) were a kind gift from Dr. Jin Ho Chung (Seoul National University, Seoul, Republic of Korea). Cells were cultured in DMEM (SH30243.01; Hyclone, South Logan, UT, USA). All media were supplemented with 10% fetal bovine serum (GenDepot, Barker, TX, USA) and 1% penicillin/streptomycin (GenDepot), and all cells were grown at 37°C in 5% CO<sub>2</sub>. The Smartvector short hairpin (sh)EPRS doxycycline-inducible knockdown cell line was established by treating lentiviral particles (EPRS mCMV-turboGFP V2IHSMCG\_687815, 687823; Dharmacon, Lafayette, CO, USA). Positive clones were enriched by treatment with 2  $\mu$ g/ml puromycin (GenDepot) and maintained in complete medium supplemented with 1  $\mu$ g/ml puromycin. The small interfering RNAs or cDNA plasmids were transiently transfected using Lipofectamine RNAiMax or Lipofectamine 3000, respectively, following the manufacturer's instructions (Thermo Fisher Scientific, Waltham, MA, USA).

### Western blot analysis

Subconfluent cells or animal tissues were harvested for whole-cell or tissue extracts using radioimmunoprecipitation assay buffer. Lysates were separated in Tris-glycine SDS-polyacrylamide gels at concentrations ranging from 8 to 12% and transferred to nitrocellulose membranes (Thermo Fisher Scientific). The target-specific antibodies used in this study are summarized

in Supplemental Table S1. The resulting Western blot images were quantified using ImageJ software [v.1.50b; National Institutes of Health (NIH), Bethesda, MD, USA]. Quantitated values were normalized using either loading control or their total forms.

### ECM deposition assay and collagen footprint assay

Control or shEPRS cells were grown on glass coverslips and treated with TGF- $\beta$ 1 or vehicle. After treatment, cells were washed in cold PBS, fixed in 4% formaldehyde in PBS, washed in PBS, and blocked in 5% bovine serum albumin in PBS. Without permeabilization, cells were incubated with collagen I or fibronectin antibody (Supplemental Table 1) overnight at 4°C, followed by an Alexa Fluor 488–conjugated secondary anti-rabbit IgG antibody (Thermo Fisher Scientific). Antibodies were diluted in 5% bovine serum albumin. DAPI was used to stain nuclei. Immunofluorescent images were acquired on a fluorescence microscope (BX51TR; Olympus, Tokyo, Japan) or on a confocal laser scanning microscope (Nikon C2; Nikon, Tokyo, Japan) as previously described (25). The fluorescence intensity was measured using ImageJ software (NIH; v.1.50b). The collagen footprint assay was conducted as previously described (26). Briefly, collagen deposition was facilitated by treating cultured cells with ascorbic acid and poly(sodium 4-styrenesulfonate) with or without TGF- $\beta$ 1. Cells were washed the following day with ice-cold PBS and lysed with 0.5% deoxycholate in PBS at 4°C with gentle agitation. The remaining collagen debris (footprint) was either immunostained for visualization or collected with 2 times SDS-PAGE sample buffer and heated at 95°C for 5 min. The collagen footprint was analyzed according to the conventional Western blotting method.

### Quantitative RT-PCR

Cells were infected or transfected to suppress the indicated genes for 24 or 48 h. Total RNA from animal tissues, cells, or 3-dimensional (3D) organoids were isolated using Qiazol Reagent (Qiagen, Hilden, Germany), and their cDNAs were synthesized using amfiRivert Platinum cDNA Synthesis Master Mix (Gen-Depot) according to the manufacturer's instructions. Quantitative RT-PCR (qRT-PCR) was performed with LaboPass™ EvaGreen Q Master (Cosmo Genetech, Seoul, Republic of Korea) and with CFX Connect Real-Time PCR (Bio-Rad, Hercules, CA, USA). The mRNA levels were normalized against glyceraldehyde 3-phosphate dehydrogenase, and CFX Maestro software (Bio-Rad) was used to analyze the data. Primers were purchased from Cosmo Genetech. The primer sequences are shown in Supplemental Table S2.

### Coimmunoprecipitation

Whole-cell lysates were prepared using immunoprecipitation lysis buffer [40 mM HEPES (pH 7.4), 150 mM NaCl, 1 mM EDTA, 0.5% Triton X-100] and precipitated with Pierce High-Capacity Streptavidin Agarose (Thermo Fisher Scientific) overnight at 4°C. Precipitates were washed 3 times with ice-cold lysis buffer and 3 times with immunoprecipitation wash buffer [40 mM HEPES (pH 7.4), 500 mM NaCl, 1 mM EDTA, 0.5% Triton X-100] and boiled in 2× SDS-PAGE sample buffer before immunoblotting.

### Luciferase assay

To analyze the promoter activity, laminin  $\gamma$ 2 (*LAMC2*) promoters (encoding regions of –1871 to +388) and *COL1A1* promoters (encoding regions of –2865 to +89) were amplified by PCR and cloned into the pGL3-basic vector. LX2 cells were seeded in 48

well plates and transfected the following day with plasmids using the Lipofectamine 3000 Transfection Reagent (Thermo Fisher Scientific).  $\beta$ -Gal was cotransfected for normalization. One day after transfection, 2 ng/ml TGF- $\beta$ 1 was added to the culture medium. After 24 h, luciferase activity was measured using the Luciferase Reporter Assay Kit (Promega, Madison, WI, USA) with a luminometer (DE/Centro LB960; Berthold Technologies, Oak Ridge, TN, USA) according to the manufacturer's instructions.

### Animal experiments

Wild-type (WT) *Eprs*<sup>+/+</sup> and *Eprs*<sup>-/-</sup> hetero-KO C57BL/6 mice were housed in a specific pathogen-free room with controlled temperature and humidity. Mouse protocols and animal experiments were approved by the Institutional Animal Care and Use Committee of Seoul National University (SNU-161201-1-3). To induce hepatic fibrosis in mice, CCl<sub>4</sub> treatment and bile duct ligation (BDL) methods were used. For the CCl<sub>4</sub>-mediated liver fibrosis model, WT and *Eprs*<sup>+/+</sup> mice aged 7 wk ( $n \geq 5$ ) were injected intraperitoneally with or without CCl<sub>4</sub> (1 mg/kg; 270652, MilliporeSigma) in 40% olive oil once a week for 5 wk. For BDL method, WT and *Eprs*<sup>-/-</sup> mice aged 10 wk ( $n = 4$ ) were anesthetized with isoflurane, and, through a midline incision, the bile duct was isolated and doubly ligated as previously described (27). Control animals underwent sham surgery. After 5 wk, mice were euthanized, and serum and tissue samples were collected for analysis. Liver samples from CCl<sub>4</sub>-treated and BDL mice were snap frozen in liquid nitrogen for Western blot, qRT-PCR, and hydroxyproline analyses or fixed in 4% formaldehyde in PBS for histologic analyses. Serum alanine transaminase (ALT), aspartate transaminase (AST), and ALP levels were measured with their respective detection slides using DRI-Chem 3500i Blood Analyzer (Fujifilm, Tokyo, Japan).

### Liver organoid culture

Mouse liver organoids were prepared from WT or *Eprs*<sup>-/-</sup> mice. Mouse livers were chopped and lysed in digestion solution containing collagenase and dispase II. Isolated ducts were collected by hand under a microscope as previously described (28) and seeded onto 3D Matrigel (10  $\mu$ g/ml; Corning, Corning, NY, USA). Cells were supplemented with culture medium containing specific growth factors as previously described (28). After 2–3 passages, organoids were differentiated. Differentiated or non-differentiated organoids were treated with 2 ng/ml TGF- $\beta$ 1 for 1 d and harvested for qRT-PCR analysis.

### Immunohistochemistry and staining

Paraffin blocks and liver tissue sections were prepared by Abion (Seoul, Republic of Korea). The sections were subjected to immunohistochemical analysis. Primary antibodies and their dilution ratios are listed in Supplemental Table S1. The Vectastain ABC-HRP Kit (Vector Laboratories, Burlingame, CA, USA) was used to visualize the stained samples. Mayer's hematoxylin (51275; MilliporeSigma) was used for counter-staining the nuclei. Masson's trichrome staining was performed by Abion. Fibrosis stage was determined according to Metavir classification separately by 2 independent scientists.

### Statistics

Statistical analyses were performed using Prism software (v.6.0; GraphPad Software, La Jolla, CA, USA). Two-way ANOVA in group analyses or Student's *t* tests were performed to determine statistical significance. A value of  $P < 0.05$  was considered statistically significant.

## RESULTS

### Suppression of EPRS in LX2 HSCs decreased the production and deposition of ECMs under TGF- $\beta$ 1 signaling

To investigate whether EPRS regulates the expression of different ECMs, including collagen I and fibronectin, a Smartvector shEPRS doxycycline-inducible knockdown LX2 cell line was established by treatment with lentiviral particles. Cell extracts were immunoblotted for mesenchymal markers of active HSCs and ECMs. Suppression of EPRS did not cause cell death, presumably because the suppression was not complete and because residual levels of EPRS were sufficient for other homeostatic functions, such as cell survival and proliferation, which would be favored by new proteins synthesized by its proline charging to prolyl-tRNA (data not shown). TGF- $\beta$ 1 treatment resulted in enhanced expression of Snail1,  $\alpha$ -smooth muscle actin ( $\alpha$ -SMA), fibronectin, and collagen I; this was abolished by suppression of EPRS (Fig. 1A). In contrast, overexpression of the PRS domain of EPRS alone in LX2 cells promoted basal ECM expression, which was further up-regulated upon TGF- $\beta$ 1 treatment (Fig. 1B). These data suggest that EPRS can up-regulate ECM expression in active LX2 HSCs.

In addition to EPRS mRNA levels, mRNA levels for diverse ECM chains, including COL1A1, COL1A2, COL4A1, FN1, and  $\alpha$ -smooth muscle actin (ACTA2), were up-regulated by TGF- $\beta$ 1 treatment; this TGF- $\beta$ 1-mediated increase in the ECM chain expression was partially blocked by suppression of EPRS (Fig. 1C). LAMC2 mRNA levels were enhanced by TGF- $\beta$ 1 but not further blocked by EPRS suppression, suggesting that the laminin  $\gamma$ 2 chain may be regulated *via* other signaling pathways and/or in different cell types. Furthermore, different levels of ECM chains were abolished by HF treatment both in EPRS-intact and EPRS-suppressed cells; however, DDIT3 (also known as CHOP) mRNA expression was enhanced by EPRS suppression and further promoted by HF treatment, indicating involvement of the AAR pathway (Fig. 1C). TGF- $\beta$ 1 had no effect on DDIT3 mRNA levels. At the protein level, HF treatment abolished TGF- $\beta$ 1-mediated and EPRS-dependent collagen I and fibronectin expression, which was partially rescued by supplementation with additional proline (Fig. 1D, lanes 3, 4, 7, 8, 11, and 12). In addition to the EPRS-dependent ECM proteins, SMAD2/3 phosphorylation and pY<sup>641</sup>STAT6 levels, with or without TGF- $\beta$ 1 treatment, were generally abolished by HF treatment but were also partially rescued by additional proline supplementation and HF treatment (Fig. 1D). COL1A1 and FN1 mRNA levels changed similarly under the same experimental conditions (Fig. 1E). However, the TGF- $\beta$ 1-mediated protein and mRNA levels of the ECMs after HF and proline treatment were still lower than those in cells treated with TGF- $\beta$ 1 alone whether EPRS level and/or activity was modulated or not (Fig. 1D, lanes 3, 4, 7, 8, 11, and 12; Fig. 1E, graphic bars 3, 4, 7, and 8). These data suggest that EPRS plays a unique role in ECM production in addition to its tRNA-charging activity, although other molecules may be involved in STAT-mediated ECM induction. Thus, EPRS

might transcriptionally regulate the expression of collagen type I and fibronectin but may not significantly regulate the expression of laminin  $\gamma$ 2.

We examined whether suppression of other aminoacyl-tRNA synthetases is involved in the regulation the ECM expression *via* analysis of the AAR pathways. Suppression of lysyl-tRNA synthetase (KRS), glycyl-tRNA synthetase (GRS), or leucyl-tRNA synthetase (LRS) led to an increase in ACTA2 mRNA upon TGF- $\beta$ 1 treatment to a level similar to nonsuppressed control LX2 cells. However, KRS-suppressed cells had DDIT3 mRNA levels that were unchanged despite TGF- $\beta$ 1 treatment compared with control cells, whereas GRS or LRS suppression increased DDIT3 levels (Supplemental Fig. S1A, B). In addition, the mRNA levels of diverse ECM chains were unchanged by suppression of any of the aminoacyl-tRNA synthetases, although TGF- $\beta$ 1 treatment promoted ECM production independent of aminoacyl-tRNA suppression (Supplemental Fig. S1C). Therefore, EPRS appeared to be involved in ECM production *via* proline-tRNA charging and non-translational mechanisms, specifically.

We examined whether the EPRS level affected the extracellular deposition and transcriptional induction of collagen I and fibronectin. Collagen I and fibronectin staining in the extracellular space of LX2 cells was more apparent upon TGF- $\beta$ 1 treatment, whereas suppression of EPRS reduced the intensity of extracellular collagen I and fibronectin staining (Fig. 1F). Furthermore, results from immunoblotting of the conditioned medium of the cells showed that suppression of EPRS reduced collagen I levels and footprint collagen I (*i.e.*, extracellularly deposited collagen I) (Fig. 1G). These observations demonstrate that EPRS up-regulated collagen and fibronectin.

The effects of EPRS expression on the regulation of ECM expression were examined using primary HFFs. TGF- $\beta$ 1 treatment up-regulated COL1A1 mRNA levels, and suppression of EPRS reduced COL1A1 mRNA levels compared with control HFFs (Supplemental Fig. S2A). HF treatment decreased TGF- $\beta$ 1-mediated COL1A1 mRNA levels compared with non-HF-treated conditions (Supplemental Fig. S2A). Again, DDIT3 mRNA levels were increased by HF treatment, suggesting activation of the AAR pathway (Supplemental Fig. S2A). Collagen I deposition outside of HFFs was much higher in EPRS-expressing parental cells than in EPRS-suppressed HFFs (Supplemental Fig. S2B–D). These results suggest that the up-regulatory effect of EPRS on ECM production and deposition can be applied to different types of mesenchymal cells.

### EPRS-mediated transcriptional regulation of ECMs involved STAT6 activation

We examined which signaling pathways or molecules could be involved in the EPRS-mediated ECM up-regulation upon TGF- $\beta$ 1 treatment. Because TGF- $\beta$ 1-mediated signaling transduces canonical SMAD-mediated signaling and noncanonical pathways, we explored molecules that are involved in both pathways. Among the molecules we tested, STATs appeared to be involved in the

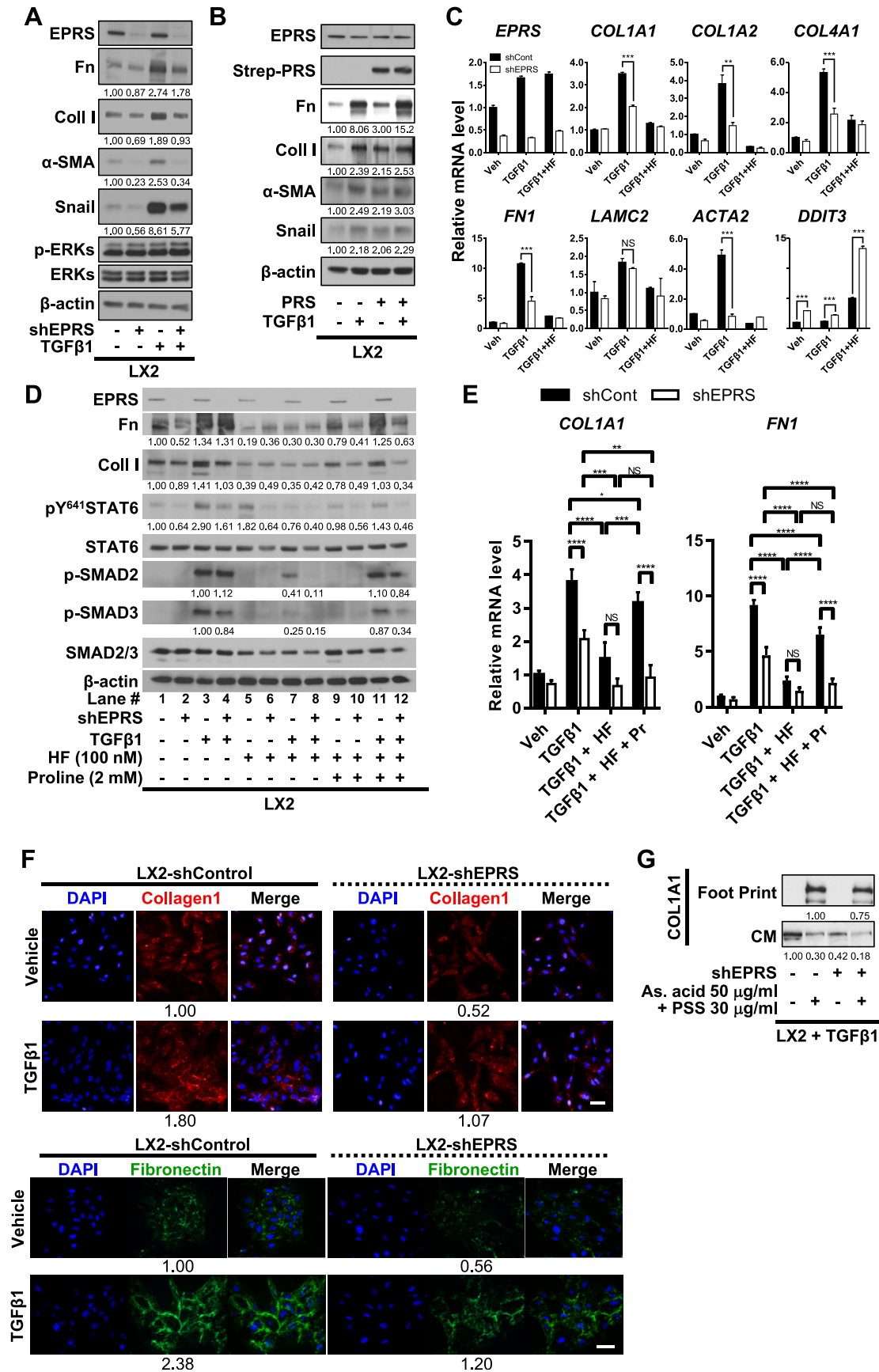


**Figure 1.** EPRS regulated expression levels of ECM chains beyond the translational process. *A, B*) Control LX2 cells, shEPRS doxycycline-inducible knockdown LX2 cell (LX2-shEPRS) (*A*) or PRS expression vector–transfected LX2 (pEXPR-103-Strep-PRS) (*B*) cells were harvested prior to immunoblotting for the indicated molecules. *C*) Subconfluent control or shEPRS-LX2 (continued on next page)

effects of TGF- $\beta$ 1; TGF- $\beta$ 1 treatment promoted the phosphorylation of STAT6 at Tyr641 (*i.e.*, pY<sup>641</sup>STAT6), and this was abolished by EPRS suppression. In contrast, phosphorylation of STAT3 at Tyr705 (*i.e.*, pY<sup>705</sup>STAT3) decreased upon EPRS suppression and was slightly reduced by TGF- $\beta$ 1 treatment (Fig. 2A). pY<sup>705</sup>STAT3 was promoted by PRS expression but was inactivated by TGF- $\beta$ 1 stimulation in LX2 cells, whereas pY<sup>641</sup>STAT6 was increased by PRS overexpression or TGF- $\beta$ 1 stimulation (Fig. 2B). In addition, we assessed whether STAT6 overexpression could promote the expression of basal or TGF- $\beta$ 1-mediated ECMs in an EPRS-dependent manner. Overexpression of STAT6 in EPRS-suppressed cells could not recover basal and TGF- $\beta$ 1-mediated pY<sup>641</sup>STAT6, fibronectin expression, and collagen I expression levels to the levels of cells with intact EPRS expression (Fig. 2C). Suppression of STAT6 decreased basal and TGF- $\beta$ 1-mediated fibronectin and collagen I expression (Fig. 2D). Thus, although sensitive to STAT6 expression, basal and TGF- $\beta$ 1-mediated ECM expression in LX2 cells appeared to depend primarily on EPRS expression. Overexpression of STAT3 did not result in a proportional relationship between pY<sup>705</sup>STAT3 and basal or TGF- $\beta$ 1-mediated collagen I expression (Fig. 2E), suggesting that STAT3 might be irrelevant to EPRS-dependent ECM production in TGF- $\beta$ 1-treated LX2 cells.

The transcriptional activity of the *COL1A1* promoter with STAT-responsive consensus elements in LX2 cells was significantly up-regulated by TGF- $\beta$ 1 treatment, but this effect was reduced with EPRS suppression (Fig. 2F, left). However, TGF- $\beta$ 1 treatment did not induce significant increases in *LAMC2* promoter activity, which was still abolished by EPRS suppression (Fig. 2F, right). Data gathered *via* qRT-PCR assays revealed that *LAMC2* mRNA levels were increased ~2-fold by TGF- $\beta$ 1 but were not significantly inhibited by EPRS suppression (Fig. 1C). This discrepancy may be due to either the effects at smaller fold changes (as shown in *y*-axis values) or different cell types; indeed, we have observed that *LAMC2* expression changed more significantly in hepatocytes than in LX2 or HSCs (unpublished results). To examine whether STAT6 was important for the EPRS-dependent transcriptional regulation of ECM chains, LX2 cells with or without STAT6 suppression were treated with vehicle or TGF- $\beta$ 1 prior to qRT-PCR analysis. *COL1A1*, *COL1A2*, *COL4A1*, *FN1*, and *ACTA2* mRNA levels were up-regulated by TGF- $\beta$ 1 treatment. Suppression of STAT6 alone was not as effective as suppression of EPRS alone, and suppression of both EPRS and STAT6 was only as effective as suppression of EPRS alone. When treated with TGF- $\beta$ 1, EPRS-intact

control cells decreased ECM mRNA levels upon additional STAT6 suppression, whereas EPRS-suppressed cells did not show any changes in ECM mRNA levels. These data suggest that EPRS could be upstream of STAT6 in TGF- $\beta$ 1-mediated ECM expression (Fig. 2G). Therefore, *LAMC2* levels were regulated by EPRS expression but were not significantly modulated by TGF- $\beta$ 1 and/or STAT6 (Fig. 2G).

### EPRS-mediated signaling occurred downstream of TGF- $\beta$ 1

We investigated how the canonical TGF- $\beta$ 1-mediated SMAD signaling pathway was involved in EPRS-dependent ECM expression. TGF- $\beta$ 1-mediated SMAD2 and SMAD3 phosphorylation was partially inhibited by EPRS suppression (Fig. 3A). Overexpression of the PRS domain alone increased basal SMAD3 phosphorylation to a saturated level that was not increased by further TGF- $\beta$ 1 treatment (Fig. 3B). In addition, TGF- $\beta$ 1-mediated pY<sup>641</sup>STAT6 was significantly increased by overexpression of SMAD3 but not of SMAD2, and this was abolished by EPRS suppression (Fig. 3C).

We examined whether TGF- $\beta$ 1-mediated signaling molecules could be involved in the phosphorylation of STATs, especially STAT6, presumably through protein-protein complexes, in an EPRS expression-dependent manner. LX2 cells were transfected with strep-tagged EPRS and treated with or without TGF- $\beta$ 1 for different periods of time. Whole-cell extracts were then prepared, and precipitation was conducted using streptavidin agarose beads for immunoblotting. Strep-EPRS was precipitated together with TGF- $\beta$ R1, Janus kinases (JAKs), and STATs, including STAT6, in a transient manner upon TGF- $\beta$ 1 treatment. KRS, but not extracellular signal-regulated kinases, was coprecipitated constitutively (Fig. 3D). Because EPRS and KRS are members of the multi-aminoacyl-tRNA synthetase complex (MSC) (29), binding of EPRS to KRS was expected. The binding of strep-EPRS to the molecules was dependent on STAT6 expression, with the exception of KRS (Fig. 3E). In addition, endogenous EPRS and TGF- $\beta$ 1-mediated pY<sup>641</sup>STAT6 coimmunoprecipitated each other, and TGF- $\beta$ R1 was found also in the immunoprecipitates (Fig. 3F). Furthermore, a point mutation in EPRS Ser999A that does not allow EPRS to dissociate from the MSC (30) maintained the ability of EPRS to form a protein complex with TGF- $\beta$ R1, SMAD3, JAKs, and STAT6 (Fig. 3G). Given the dynamic dimerization among STATs (31), the TGF- $\beta$ R1-STAT6 complex could include other STATs.

cells were treated with TGF- $\beta$ 1 (2 ng/ml) with or without HF (100 nM) for 24 h before qRT-PCR analysis. Data are means  $\pm$  sd. NS, nonsignificant. \*\* $P$  < 0.01, \*\*\* $P$  < 0.001 (Student's *t* test). *D*, *E*) Control LX2 or shEPRS-LX2 cells were treated with TGF- $\beta$ 1, HF (100 nM), and/or proline (2 mM) for 24 h prior to preparation of whole-cell extracts for immunoblotting (*D*) or qRT-PCR (*E*) for the indicated molecules. NS, nonsignificant. \* $P$  < 0.05, \*\* $P$  < 0.01, \*\*\* $P$  < 0.001, \*\*\*\* $P$  < 0.0001 (2-way ANOVA). *F*) LX2 (LX2-shControl or LX2-shEPRS) cells on coverglasses were stained for DAPI (for DNA, blue) and collagen I (red, top panel) or fibronectin (green, bottom panel). Relative fluorescence intensities of ECMs are displayed under the images. Scale bars, 60  $\mu$ m. *G*) LX2-control (-) or LX2-shEPRS (shEPRS, +) cells were treated with ascorbic acid (50  $\mu$ g/ml) and poly(sodium 4-styrenesulfonate) (PSS; 30  $\mu$ g/ml) for 24 h along with TGF- $\beta$ 1 (2 ng/ml). Conditioned medium (CM) or footprint extracts (with deposited ECM proteins) were then prepared for immunoblotting against *COL1A1*. Data represent 3 independent experiments.

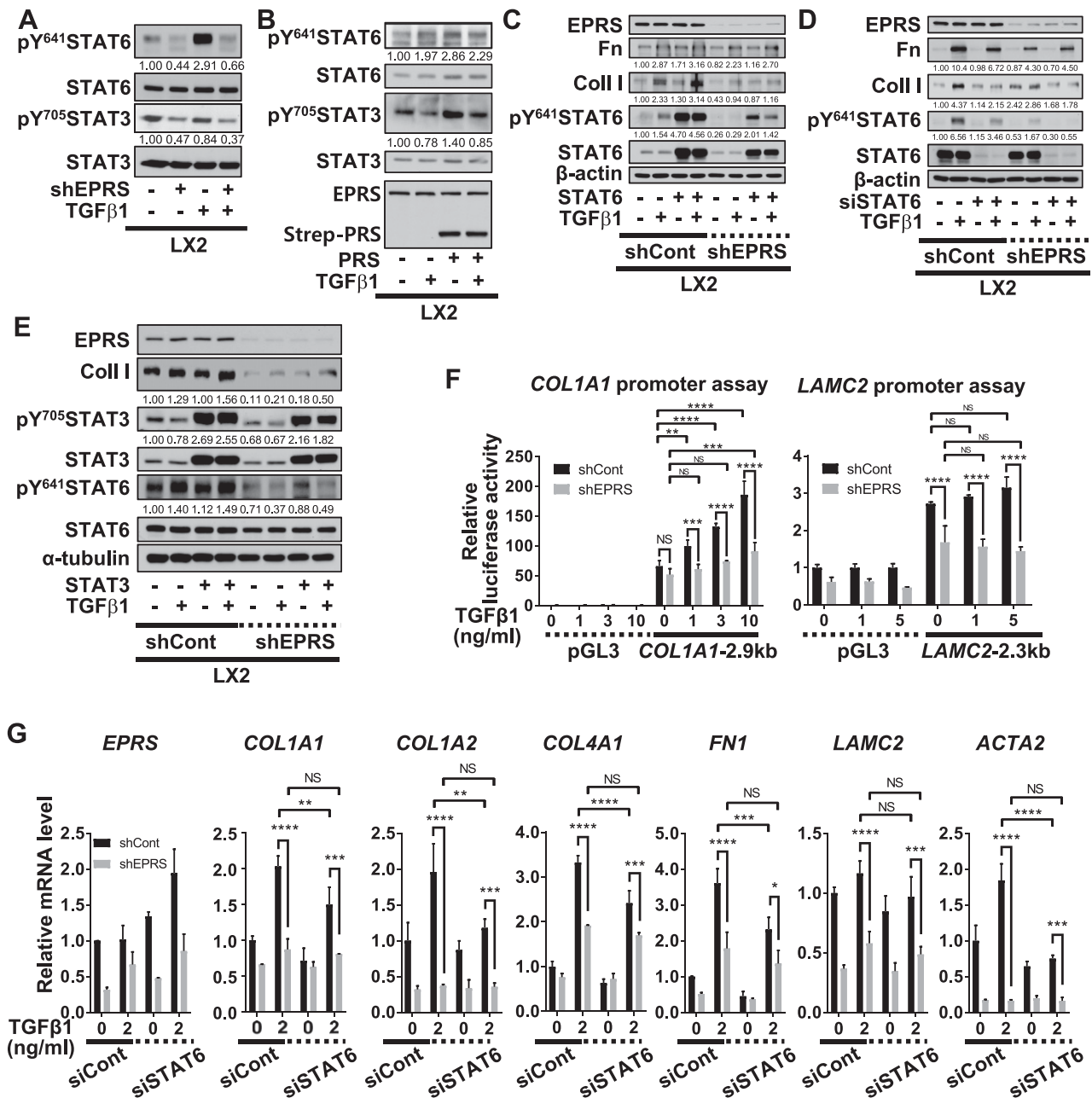


**Figure 2.** STAT6 phosphorylation upon TGF-β1 treatment to LX2 cells was required for ECM production. *A–E*) LX2 cells were stably infected with the control (–) or shEPRS virus (LX2-shEPRS). Control LX2 cells were transiently transfected with different expression vectors, as indicated, in the absence (–) or presence of TGF-β1 (2 ng/ml, +) for 24 h, followed by whole-cell extract preparation and immunoblotting for the indicated molecules. *F*) LX2 cells transfected with *COL1A1* or *LAMC2* promoter luciferase constructs with STATs-consensus responsive sequences (*COL1A1*-2.9 kb and *LAMC2*-2.3 kb constructs with upstream promoter regions up to –2.9 and –2.3 kb, respectively) were treated with TGF-β1 at the indicated concentrations for 24 h prior to luciferase reporter analysis. *G*) Subconfluent control LX2 cells were transiently transfected with small interfering RNA against a control sequence (siCont) or STAT6 (siSTAT6) in the absence (0) or presence of TGF-β1 (2 ng/ml) treatment for 24 h, followed by qRT-PCR analysis. Data are presented as means ± SD. Data represent 3 isolated experiments. NS, nonsignificant. \**P* < 0.05, \*\**P* < 0.01, \*\*\**P* < 0.001, \*\*\*\**P* < 0.0001 (Student's *t* test).

### ***In vivo* liver tissues from fibrotic mice showed EPRS-dependent STAT6 phosphorylation and ECM production**

To investigate the physiologic roles of EPRS in *in vivo* animal models of liver fibrosis, normal WT (*Eprs*<sup>+/+</sup>) and *Eprs*<sup>-/+</sup> hetero-knockout (KO) mice were treated with CCl<sub>4</sub>. Expression of ECMs, including fibronectin, collagen

I, and laminins, increased in WT mice with CCl<sub>4</sub> treatment compared with untreated mice (Fig. 4A). However, CCl<sub>4</sub> treatment of *Eprs*<sup>-/+</sup> mice showed less-significant increases in fibronectin and collagen I expression without affecting laminin levels (Fig. 4A). Concomitantly, pY<sup>641</sup>STAT6 was increased in WT mice upon CCl<sub>4</sub> treatment compared with *Eprs*<sup>-/+</sup> mice (Fig. 4A). α-SMA levels, pY<sup>701</sup>STAT1, and pY<sup>705</sup>STAT3 were not dependent on



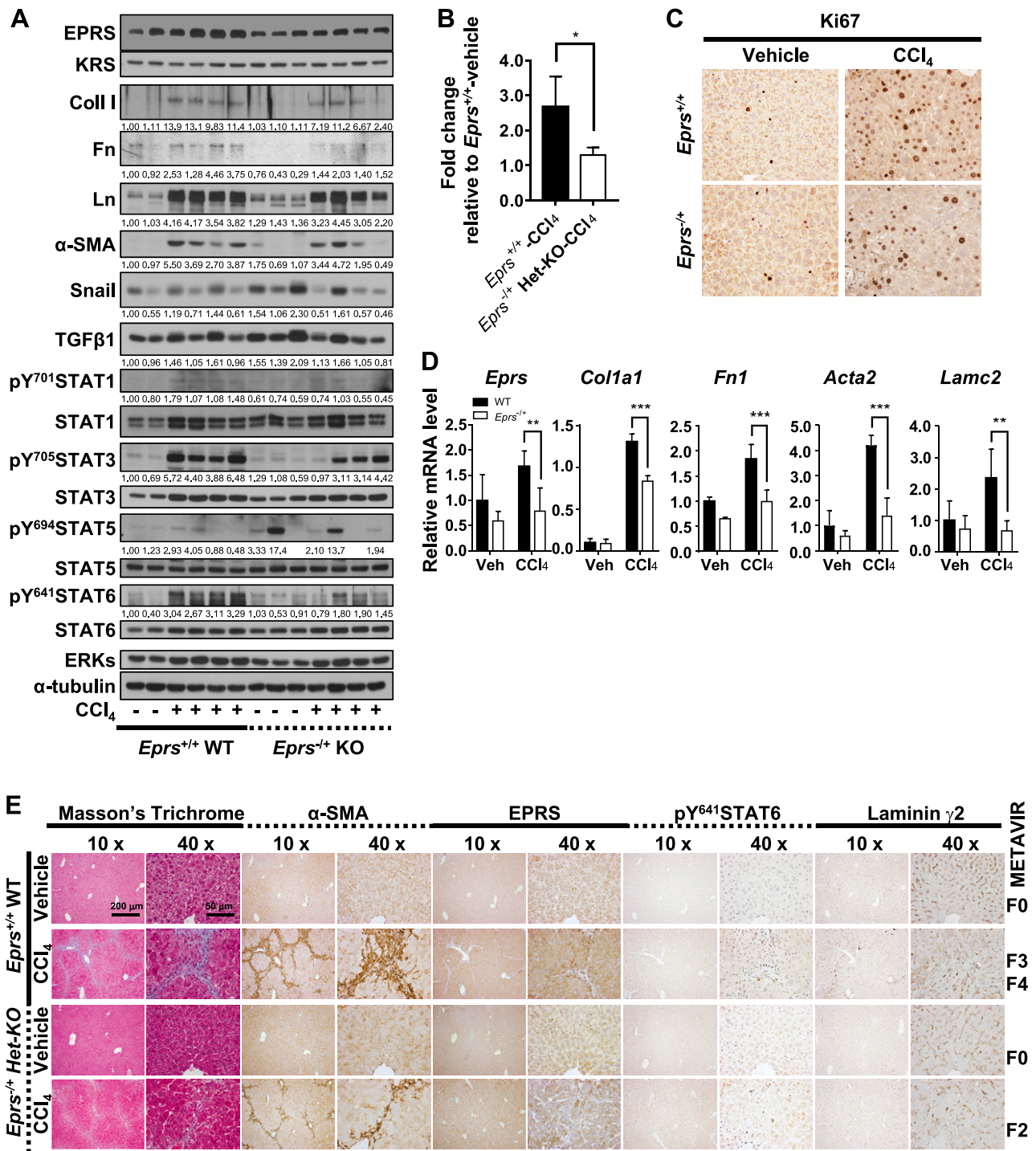


**Figure 4.** CCl<sub>4</sub>-treated mice showed EPRS-dependent ECM production. WT (*Eprs*<sup>+/+</sup>) and *Eprs*<sup>-/-</sup> hetero-KO C57BL/6 mice were treated with vehicle or CCl<sub>4</sub> (1 mg/kg in 40% olive oil) once a week for 5 wk. *A–D*) Liver tissue extracts were prepared and processed for immunoblotting (*A*), the hydroxyproline assay (*B*), immunohistochemistry using anti-Ki67 antibody (*C*), and qRT-PCR (*D*). Data are presented as means ± SD. \**P* < 0.05, \*\**P* < 0.01, \*\*\**P* < 0.001 (Student's *t* test). *E*) Liver tissues were processed for Masson's trichrome staining or immunohistochemistry, followed by image capturing at ×10 (scale bar, 200 μm) and ×40 (scale bar, 50 μm) magnification. Fibrotic grade according to the Metavir scores are indicated on the right side. Data represent 3 different experiments.

EPRS expression, and pY<sup>694</sup>STAT5 level was not affected by EPRS expression (Fig. 4A). These observations suggest that EPRS-dependent ECM expression may involve STAT6 activation. Furthermore, CCl<sub>4</sub>-treated WT mice showed higher amounts of collagen I in liver extracts

compared with CCl<sub>4</sub>-treated *Eprs*<sup>-/-</sup> mice (Fig. 4B). CCl<sub>4</sub> treatment of *Eprs*<sup>+/+</sup> or *Eprs*<sup>-/-</sup> mice increased Ki67 levels as measured by immunostaining, although the amount of Ki67 in *Eprs*<sup>-/-</sup> mice livers might be comparable to, or slightly lower than, that of *Eprs*<sup>+/+</sup> mice livers (Fig. 4C),

indicating that hetero-KO of *Eprs* did not significantly affect cell proliferation after CCl<sub>4</sub> treatment. Consistently, the mRNA levels of collagen I  $\alpha$ 1 chain (*Col1a1*), *Fn1*, *Lamc2*, and *Acta2* were dramatically up-regulated by CCl<sub>4</sub> treatment in the livers of WT mice. CCl<sub>4</sub> treatment did not show significant effects in the livers of *Eprs*<sup>-/+</sup> mice (Fig. 4D).

We then analyzed the liver tissues by immunostaining for different molecules. CCl<sub>4</sub> administration to *Eprs*<sup>+/+</sup> control mice caused septal fibrosis or cirrhosis with intense collagen I deposition or  $\alpha$ -SMA/HSC activation along septa (F3 and F4 of METAVIR score). In WT mice, treatment with CCl<sub>4</sub> increased collagen I deposition as visualized using Masson's trichrome staining. Activation of  $\alpha$ -SMA (presumably in HSCs) staining along scars, pY<sup>641</sup>STAT6 stains at nuclear regions, and laminin  $\gamma$ 2 immunostaining were enhanced (Fig. 4E). Mice without CCl<sub>4</sub> treatment did not show the fibrotic phenotypes (F0 of METAVIR score). However, CCl<sub>4</sub> treatment of *Eprs*<sup>-/+</sup> hetero-KO mice led to delayed or less-developed fibrotic phenotypes of portal fibrosis with few septa (F2 of Metavir score) (Fig. 4E), suggesting that CCl<sub>4</sub>-mediated fibrotic phenotypes in livers are EPRS dependent. In addition, laminin  $\gamma$ 2 immunostains could be differentiated from collagen I stains, suggesting that different cell types might be involved.

We adapted the liver fibrosis model using a BDL approach. WT *Eprs*<sup>+/+</sup> and *Eprs*<sup>-/+</sup> mice were processed to BDL operation. Five weeks later, analysis showed that BDL increased the activity of AST, ALT, and ALP in animal sera (Fig. 5A). The levels of AST and ALT, which are indicative of fibrotic liver damage, were significantly higher in *Eprs*<sup>+/+</sup> BDL mice compared with *Eprs*<sup>-/+</sup> mice. However, ALP activity levels did not show significant changes between *Eprs*<sup>+/+</sup> and *Eprs*<sup>-/+</sup> mice after BDL. Whereas *Eprs*<sup>+/+</sup> mice showed enhanced fibronectin expression and pY<sup>641</sup>STAT6 levels after BDL, *Eprs*<sup>-/+</sup> mice showed much reduced ECM expression and pY<sup>641</sup>STAT6 levels (Fig. 5B). In addition, *Acta2*, *Col1a1*, and *Fn1* mRNA levels were less increased by BDL in liver tissues of *Eprs*<sup>-/+</sup> mice compared with those of *Eprs*<sup>+/+</sup> mice (Fig. 5C). Further, immunohistochemistry and Masson's trichrome staining for collagen I synthesis showed that BDL of *Eprs*<sup>+/+</sup> mice led to increases in  $\alpha$ -SMA, pY<sup>641</sup>STAT6, and collagen I, whereas BDL of *Eprs*<sup>-/+</sup> mice showed less of this effect; BDL of *Eprs*<sup>+/+</sup> mice resulted in severe fibrotic levels (F3 of Metavir score), but BDL of *Eprs*<sup>-/+</sup> mice resulted in F2 fibrotic level, although all control mice (without BDL) showed no phenotype (F0 of Metavir score) (Fig. 5D). This alternative model of liver fibrosis showed that EPRS could play an important role in hepatic fibrogenesis.

### Liver organoids in a 3D Matrigel system revealed EPRS-dependent regulation of ECM induction

We prepared liver organoids from ductal stem cells of WT and *Eprs*<sup>-/+</sup> mice and used 3D Matrigels to examine EPRS-dependent ECM induction. Differentiated liver organoids showed increased albumin (*Alb*) mRNA, which is an

indicator of hepatocyte differentiation. TGF- $\beta$ 1 treatment reduced *Alb* mRNA levels and increased *Fn1* mRNA levels. In contrast, *Eprs*<sup>-/+</sup> liver organoids showed lower *Fn1* levels, and *Alb* mRNA levels were unchanged (Fig. 6A). Although *Eprs* mRNA expression was not important for liver organoid growth and TGF- $\beta$ 1-mediated differentiation, *Fn1* mRNA levels were greatly dependent on *Eprs* expression and TGF- $\beta$ 1 treatment (Fig. 6A). *Col1a1* mRNA expression did not significantly depend on *Eprs* expression, although *Lamc2* mRNA levels appeared slightly dependent on TGF- $\beta$ 1 treatment and *Eprs* expression (Fig. 6B). Similar to our finding in LX2 cells and mouse models, the TGF- $\beta$ 1-mediated transcriptional induction of fibronectin depended on EPRS expression. However, collagen I expression was dependent on EPRS in LX2 cells and animal models but not in liver organoids.

## DISCUSSION

This study demonstrates that EPRS transcriptionally regulated the expression of ECMs, including collagen I and fibronectin, via TGF- $\beta$ 1-mediated signaling pathways involving a formation of complexes among TGF- $\beta$ R1, SMAD3, JAKs, and STAT6. Furthermore, a TGF- $\beta$ 1-mediated signaling pathway targeted toward STAT6 was observed in a CCl<sub>4</sub>-mediated liver fibrosis animal model, leading to ECM induction (Fig. 6C). Thus, this study suggests that EPRS can be a promising antifibrotic target.

Among *in vitro* LX2 HSCs, CCl<sub>4</sub>-treated animal liver tissues, and 3D organoid models, the dependency of ECM chains levels on EPRS expression could be differential, presumably depending on cell type and/or the signaling context involved in the experimental models. Fibronectin was clearly shown to be expressed in an EPRS-dependent manner in all 3 models. Collagen I expression depended on EPRS in LX2 and animal models, but laminin  $\gamma$ 2 only slightly depended on EPRS in the liver organoid model. Compared with collagen I, which has been shown to be a main component in fibrotic livers, laminin  $\gamma$ 2 is a biomarker of acute lung injury (32) and an HCC biomarker in the sera of patients with HCC (33). Thus, laminin  $\gamma$ 2 may also be important for the progression of precancerous liver pathology to HCC. However, the regulation of laminin  $\gamma$ 2 expression differed among the 3 study models. In addition, we observed that  $\alpha$ -SMA-positive HSCs were responsible for collagen I expression, whereas albumin-positive hepatocytes could be responsible for laminin  $\gamma$ 2 expression in CCl<sub>4</sub>-treated fibrotic mouse livers (data not shown).

HF is a competitive inhibitor of EPRS activity (10) and reduces TGF- $\beta$ -mediated collagen synthesis in humans (16). Its antifibrotic effects appear to involve influences on TGF- $\beta$ 1/SMAD3 signaling activity and other signaling molecules, depending on cell types (18). Moreover, prevention of Th17 cell differentiation leads to the inhibition of autoimmune inflammation (19). HF is highly efficacious in inhibiting fibrosis (34), but it causes significant side effects characterized by severe gastrointestinal lesions and hemorrhage (35). The antagonistic effects of HF on SMAD3 phosphorylation can be at least partially due to

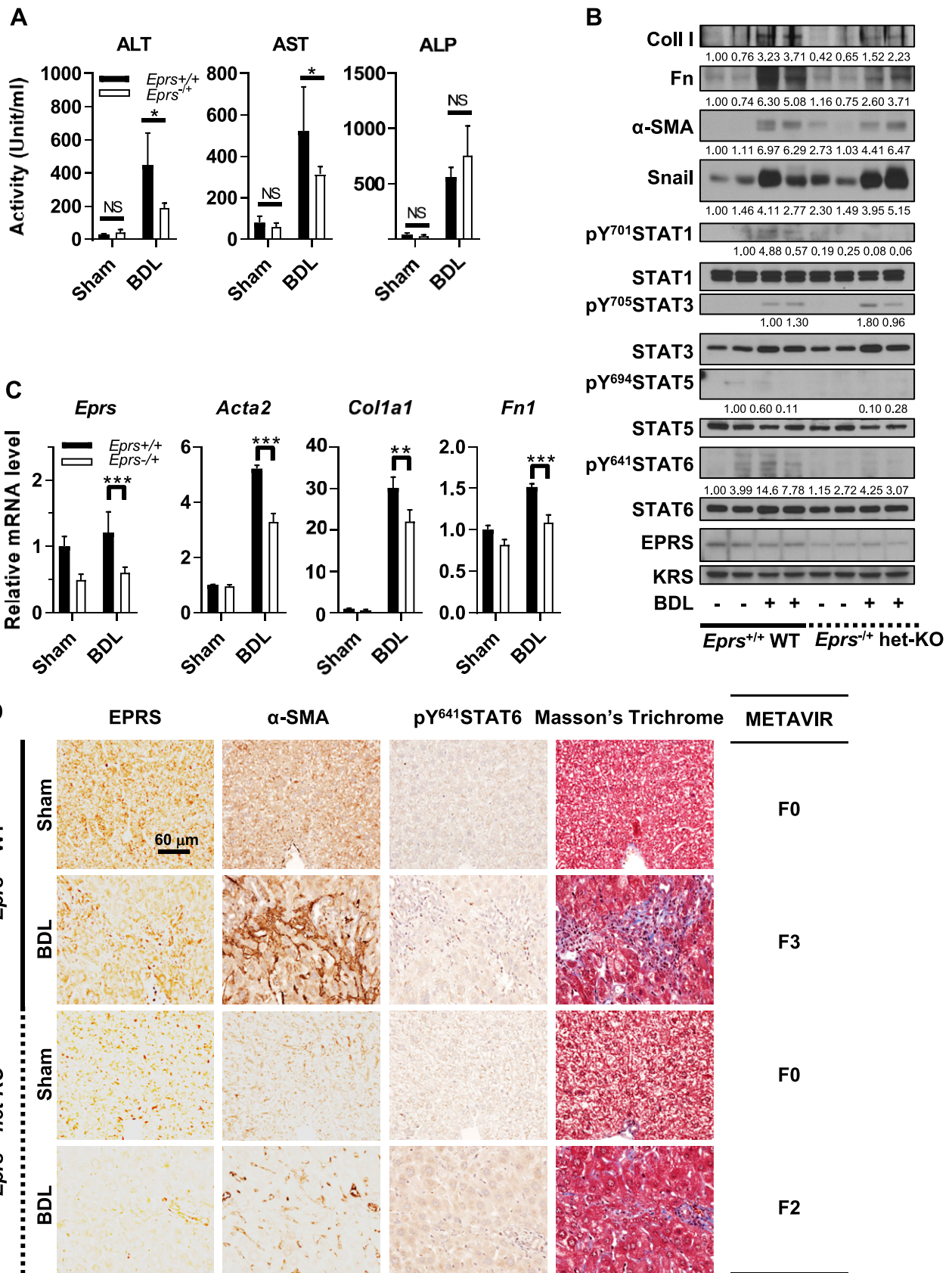


**Figure 5.** BDL model in mice showed EPRS-dependent ECM production. *A–D*) WT (*Eprs*<sup>+/+</sup>) and *Eprs*<sup>-/+</sup> hetero-KO C57BL/6 mice underwent sham surgery, or their bile ducts were ligated for 5 wk. *A*) Serum levels of ALT, AST, and ALP were measured. *B*, *C*) Liver tissue extracts were prepared and processed for immunoblotting (*B*) and qRT-PCR (*C*). Data are presented as means ± SD. NS, nonsignificant. \**P* < 0.05, \*\**P* < 0.01, \*\*\**P* < 0.001 (Student's *t* test). *D*) Liver tissues were processed for Masson's trichrome staining or immunohistochemistry followed by imaging at ×40 magnification. Scale bar, 60 μm. Fibrotic grades according to the Metavir scores are indicated in the right side. Data represent 3 different experiments.

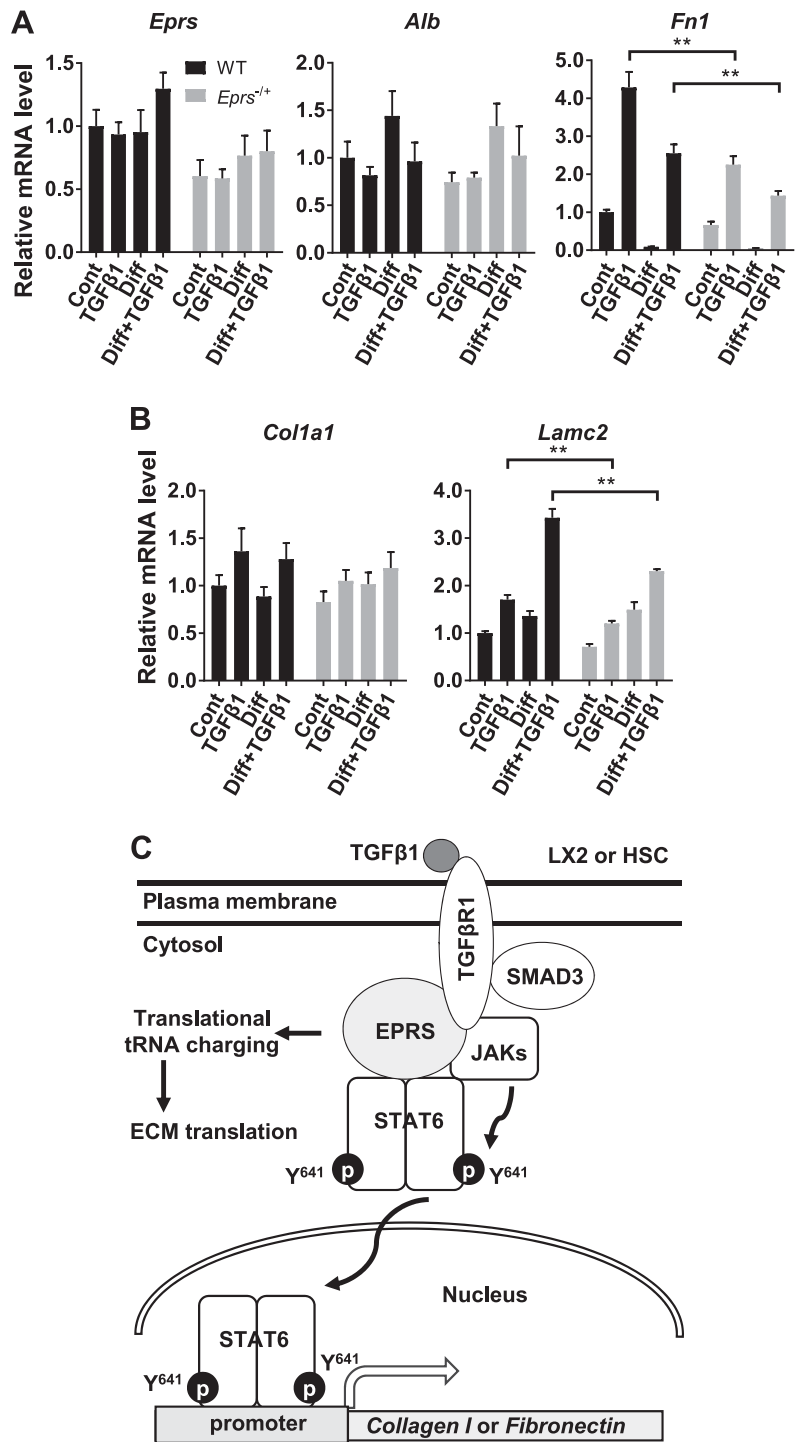


**Figure 6.** Liver organoid models prepared from WT or *Eprs*<sup>+/-</sup> hetero-KO mice also showed EPRS-dependent fibronectin expression. *A, B*) Organoid cultures after the embedding of ductal cells prepared from WT *Eprs*<sup>+/-</sup> or *Eprs*<sup>+/-</sup> hetero-KO mouse livers into 3D Matrigel were treated with TGF-β1 (2 ng/ml) before or after differentiation processes (diff.). After 24 h, the organoids were harvested and processed for qRT-PCR for the indicated molecules. Data are means ± sd. Data shown represent 3 independent experiments. \*\**P* < 0.01 (Student's *t* test). *C*) The working model for EPRS-dependent ECM expression on TGF-β1 treatment to LX2 cells. TGF-β1 treatment leads to formation of protein complex among TGF-β1R, SMAD3, EPRS, JAKs, and pY<sup>641</sup>STAT6. Active pY<sup>641</sup>STAT6 causes transcriptional activations of the promoters of *COL1A1* or *FN1* genes. In addition, EPRS can play role in translational charging of prolyl-tRNAs during ECM expression.

the HF-mediated activation of other signaling molecules, including AKT serine/threonine kinases, extracellular signal-regulated kinases, and p38 mitogen-activated protein kinase phosphorylation (36). As a multifunctional cytokine, TGF-β1 plays significant roles in several biologic activities encompassing various effectors and receptors (37). Thus, it is likely that HF causes side effects by targeting TGF-β signaling that is also important for homeostatic immune and inflammatory functions (18, 22). Therefore, more studies are needed to develop safer anti-fibrotic reagents that can target specific EPRS- and/or

TGF-β1-mediated signaling components of pathways leading to ECM production.

The biologic activity of HF also involves the inhibition of proline utilization by EPRS (10). EPRS is traditionally important for loadings of proline to tRNA<sup>Pro</sup> during amino acid polymerization following the codon information on mRNA. Although the α1 chain of collagen I includes a proline composition of 19.0%, this study revealed that EPRS could also regulate the mRNA expression of *COL1A1* and *FN1* (with a lower 7.9% proline content). Furthermore, in EPRS-suppressed cells, proline enrichment

could not recover the inhibitory effect of HF on ECM production, thereby indicating another role of EPRS in ECM production beyond proline-charging to tRNA<sup>Pro</sup>. Additionally, EPRS expression was positively correlated with the extracellular deposition of collagen I, suggesting that EPRS can play positive roles in the synthesis of ECMs.

It was recently reported that TGF- $\beta$ 1 can interact with JAK1, leading to early STAT3 phosphorylation in normal hepatocytes or hepatic cancer cells (38). In our study, STAT3 expression did not enhance ECM expression in TGF- $\beta$ 1-treated LX2 HSCs. STAT3 also negatively responded to TGF- $\beta$ 1 stimulation but was positively correlated with EPRS expression. In contrast, STAT6 phosphorylation was correlated with the up-regulatory effects of EPRS and with the TGF- $\beta$ 1 effects on collagen I and fibronectin expression. Thus, it is likely that different hepatic cell types can adapt different forms of STATs downstream of TGF- $\beta$ 1 stimulation. Results from this study also show that EPRS may be a component of the TGF- $\beta$ 1/SMAD3-mediated protein complex consisting of JAKs and STATs.

EPRS is also a component for the cytosolic MSC. Once EPRS is phosphorylated at Ser999 by mTORC1-S6K1, EPRS can be dissociated from the MSC and translocate to the membrane, where it can interact with fatty acid transporter upon insulin stimulation to adipocytes (30). Thus, EPRS can translocate to the plasma membrane. However, the current study shows that phosphorylation of EPRS at Ser999 in LX2 HSCs was not required for TGF- $\beta$ 1 binding. The discrepancy in the requirement of EPRS phosphorylation at Ser999 to translocate from the cytosolic MSC to membrane might be due to differences in cell types and/or signaling contexts. Alternatively, it cannot be ruled out that EPRS, as a component of MSC, may have the capacity to bind to TGF- $\beta$ 1. Overall, results from this study suggest that it may be reasonable to target the EPRS-dependent, TGF- $\beta$ 1-STAT6 signaling axis to inhibit fibrotic ECM production. **FJ**

## ACKNOWLEDGMENTS

The authors thank Dr. Myung Hee Kim (Korea Research Institute of Bioscience and Biotechnology) for EPRS constructs, Dr. Scott Friedman (Ichan School of Medicine, Mount Sinai, New York, NY, USA) for LX2 cells, and Dr. Jin Ho Chung (Seoul National University) for HFFs. This work was supported by Korea Institute of Science and Technology Gangneung Institute Intramural Research Grant 2Z05310 (to C.-H.P. and D.-G.S.); Basic Science Research Program through the National Research Foundation of Korea (NRF) (funded by the Ministry of Science); Information and Communications Technology (ICT) and Future Planning Grants NRF-2018M3A9C8020027 and NRF-2017RIA2B3005015; Tumor Microenvironment Global Core Research Center (GCRC) Grant 2011-0030001; and Medicinal Bioconvergence Research Center Grant NRF-2013M3A6A4044019 (to J.W.L.). The authors declare no conflicts of interest.

## AUTHOR CONTRIBUTIONS

D.-G. Song performed most experiments; D. Kim and S. Kim helped with the animal study; J. H. Kim and S. Kim helped with the experimental reagents; J. W. Jung, S. H. Nam, J. E. Kim, and H.-J. Kim helped with the imaging

experiments or with reagents; S.-J. Lee helped with the extracellular collagen deposition experiments; C.-H. Pan, S. Kim, and J. W. Lee discussed the data; and J. W. Lee wrote the manuscript.

## REFERENCES

- Gressner, O. A., and Gao, C. (2014) Monitoring fibrogenic progression in the liver. *Clin. Chim. Acta* **433**, 111–122
- Schuppan, D., Ashfaq-Khan, M., Yang, A. T., and Kim, Y. O. (2018) Liver fibrosis: direct antifibrotic agents and targeted therapies. *Matrix Biol.* **68–69**, 435–451
- Huang, Y., Deng, X., and Liang, J. (2017) Modulation of hepatic stellate cells and reversibility of hepatic fibrosis. *Exp. Cell Res.* **352**, 420–426
- Gressner, A. M., and Weiskirchen, R. (2006) Modern pathogenetic concepts of liver fibrosis suggest stellate cells and TGF-beta as major players and therapeutic targets. *J. Cell. Mol. Med.* **10**, 76–99
- Maher, J. J., and McGuire, R. F. (1990) Extracellular matrix gene expression increases preferentially in rat lipocytes and sinusoidal endothelial cells during hepatic fibrosis in vivo. *J. Clin. Invest.* **86**, 1641–1648
- Karsdal, M. A., Manon-Jensen, T., Genovese, F., Kristensen, J. H., Nielsen, M. J., Sand, J. M., Hansen, N. U., Bay-Jensen, A. C., Bager, C. L., Krag, A., Blanchard, A., Krarup, H., Leeming, D. J., and Schuppan, D. (2015) Novel insights into the function and dynamics of extracellular matrix in liver fibrosis. *Am. J. Physiol. Gastrointest. Liver Physiol.* **308**, G807–G830
- Hynes, R. O., and Naba, A. (2012) Overview of the matrisome: an inventory of extracellular matrix constituents and functions. *Cold Spring Harb. Perspect. Biol.* **4**, a004903
- Li, X., Zhu, L., Wang, B., Yuan, M., and Zhu, R. (2017) Drugs and targets in fibrosis. *Front. Pharmacol.* **8**, 855
- Tu, T., Calabro, S. R., Lee, A., Maczurek, A. E., Budzinska, M. A., Warner, F. J., McLennan, S. V., and Shackel, N. A. (2015) Hepatocytes in liver injury: victim, bystander, or accomplice in progressive fibrosis? *J. Gastroenterol. Hepatol.* **30**, 1696–1704
- Keller, T. L., Zocco, D., Sundrud, M. S., Hendrick, M., Edenius, M., Yum, J., Kim, Y. J., Lee, H. K., Cortese, J. F., Wirth, D. F., Dignam, J. D., Rao, A., Yeo, C. Y., Mazitschek, R., and Whitman, M. (2012) Halofuginone and other febrifugine derivatives inhibit poly(tRNA) synthetase. *Nat. Chem. Biol.* **8**, 311–317
- Thiaville, M. M., Dudenhausen, E. E., Zhong, C., Pan, Y. X., and Kilberg, M. S. (2008) Deprivation of protein or amino acid induces C/EBPbeta synthesis and binding to amino acid response elements, but its action is not an absolute requirement for enhanced transcription. *Biochem. J.* **410**, 473–484
- Lu, P. D., Harding, H. P., and Ron, D. (2004) Translation reinitiation at alternative open reading frames regulates gene expression in an integrated stress response. *J. Cell Biol.* **167**, 27–33
- Bruhagat, A., Jousse, C., Wang, X. Z., Ron, D., Ferrara, M., and Fafournoux, P. (1997) Amino acid limitation induces expression of CHOP, a CCAAT/enhancer binding protein-related gene, at both transcriptional and post-transcriptional levels. *J. Biol. Chem.* **272**, 17588–17593
- Harding, H. P., Zhang, Y., Zeng, H., Novoa, I., Lu, P. D., Calfon, M., Sadri, N., Yun, C., Popko, B., Paules, R., Stojdl, D. F., Bell, J. C., Hettmann, T., Leiden, J. M., and Ron, D. (2003) An integrated stress response regulates amino acid metabolism and resistance to oxidative stress. *Mol. Cell* **11**, 619–633
- Ghosh, A. K., Quaggin, S. E., and Vaughan, D. E. (2013) Molecular basis of organ fibrosis: potential therapeutic approaches. *Exp. Biol. Med. (Maywood)* **238**, 461–481
- Halevy, O., Nagler, A., Levi-Schaffer, F., Genina, O., and Pines, M. (1996) Inhibition of collagen type I synthesis by skin fibroblasts of graft versus host disease and scleroderma patients: effect of halofuginone. *Biochem. Pharmacol.* **52**, 1057–1063
- Turgeman, T., Hagai, Y., Huebner, K., Jassal, D. S., Anderson, J. E., Genin, O., Nagler, A., Halevy, O., and Pines, M. (2008) Prevention of muscle fibrosis and improvement in muscle performance in the mdx mouse by halofuginone. *Neuromuscul. Disord.* **18**, 857–868
- Luo, Y., Xie, X., Luo, D., Wang, Y., and Gao, Y. (2017) The role of halofuginone in fibrosis: more to be explored? *J. Leukoc. Biol.* **102**, 1333–1345

19. Zhou, H., Sun, L., Yang, X. L., and Schimmel, P. (2013) ATP-directed capture of bioactive herbal-based medicine on human tRNA synthetase. *Nature* **494**, 121–124
20. Kaiser, E., Hu, B., Becher, S., Eberhard, D., Schray, B., Baack, M., Hameister, H., and Knippers, R. (1994) The human EPRS locus (formerly the QARS locus): a gene encoding a class I and a class II aminoacyl-tRNA synthetase. *Genomics* **19**, 280–290
21. Pines, M., and Spector, I. (2015) Halofuginone: the multifaceted molecule. *Molecules* **20**, 573–594
22. Luzina, I. G., Todd, N. W., Sundararajan, S., and Atamas, S. P. (2015) The cytokines of pulmonary fibrosis: much learned, much more to learn. *Cytokine* **74**, 88–100
23. Choi, S., Lee, S.-A., Kwak, T. K., Kim, H. J., Lee, M. J., Ye, S.-K., Kim, S.-H., Kim, S., and Lee, J. W. (2009) Cooperation between integrin  $\alpha 5$  and tetraspan TM4SF5 regulates VEGF-mediated angiogenic activity. *Blood* **113**, 1845–1855
24. Lee, M.-S., Kim, T. Y., Kim, Y.-B., Lee, S.-Y., Ko, S.-G., Jong, H.-S., Kim, T.-Y., Bang, Y.-J., and Lee, J. W. (2005) The signaling network of transforming growth factor  $\beta 1$ , protein kinase Cdelta, and integrin underlies the spreading and invasiveness of gastric carcinoma cells. *Mol. Cell. Biol.* **25**, 6921–6936
25. Kim, H. J., Kwon, S., Nam, S. H., Jung, J. W., Kang, M., Ryu, J., Kim, J. E., Cheong, J. G., Cho, C. Y., Kim, S., Song, D. G., Kim, Y. N., Kim, T. Y., Jung, M. K., Lee, K. M., Pack, C. G., and Lee, J. W. (2017) Dynamic and coordinated single-molecular interactions at TM4SF5-enriched microdomains guide invasive behaviors in 2- and 3-dimensional environments. *FASEB J.* **31**, 1461–1481
26. Lareu, R. R., Subramhanya, K. H., Peng, Y., Benny, P., Chen, C., Wang, Z., Rajagopalan, R., and Raghunath, M. (2007) Collagen matrix deposition is dramatically enhanced in vitro when crowded with charged macromolecules: the biological relevance of the excluded volume effect. *FEBS Lett.* **581**, 2709–2714
27. Tag, C. G., Sauer-Lehnen, S., Weiskirchen, S., Borkham-Kamphorst, E., Tolba, R. H., Tacke, F., and Weiskirchen, R. (2015) Bile duct ligation in mice: induction of inflammatory liver injury and fibrosis by obstructive cholestasis. *J. Vis. Exp.* **96**, 52438
28. Broutier, L., Andersson-Rolf, A., Hindley, C. J., Boj, S. F., Clevers, H., Koo, B. K., and Huch, M. (2016) Culture and establishment of self-renewing human and mouse adult liver and pancreas 3D organoids and their genetic manipulation. *Nat. Protoc.* **11**, 1724–1743
29. Park, S. G., Schimmel, P., and Kim, S. (2008) Aminoacyl tRNA synthetases and their connections to disease. *Proc. Natl. Acad. Sci. USA* **105**, 11043–11049
30. Arif, A., Terenzi, F., Potdar, A. A., Jia, J., Sacks, J., China, A., Halawani, D., Vasu, K., Li, X., Brown, J. M., Chen, J., Kozma, S. C., Thomas, G., and Fox, P. L. (2017) EPRS is a critical mTORC1-S6K1 effector that influences adiposity in mice. *Nature* **542**, 357–361
31. Delgoffe, G. M., and Vignali, D. A. (2013) STAT heterodimers in immunity: a mixed message or a unique signal? *JAK-STAT* **2**, e23060
32. Katayama, M., Ishizaka, A., Sakamoto, M., Fujishima, S., Sekiguchi, K., Asano, K., Betsuyaku, T., Kotani, T., Ware, L. B., Matthay, M. A., and Hashimoto, S. (2010) Laminin gamma2 fragments are increased in the circulation of patients with early phase acute lung injury. *Intensive Care Med.* **36**, 479–486
33. Kiyokawa, H., Yasuda, H., Oikawa, R., Okuse, C., Matsumoto, N., Ikeda, H., Watanabe, T., Yamamoto, H., Itoh, F., Otsubo, T., Yoshimura, T., Yoshida, E., Nakagawa, M., Koshikawa, N., and Seiki, M. (2017) Serum monomeric laminin- $\gamma 2$  as a novel biomarker for hepatocellular carcinoma. *Cancer Sci.* **108**, 1432–1439
34. McLaughlin, N. P., Evans, P., and Pines, M. (2014) The chemistry and biology of febrifugine and halofuginone. *Bioorg. Med. Chem.* **22**, 1993–2004
35. Jiang, S., Zeng, Q., Gettayacamin, M., Tungtaeng, A., Wannaying, S., Lim, A., Hansukjariya, P., Okunji, C. O., Zhu, S., and Fang, D. (2005) Antimalarial activities and therapeutic properties of febrifugine analogs. *Antimicrob. Agents Chemother.* **49**, 1169–1176
36. Roffe, S., Hagai, Y., Pines, M., and Halevy, O. (2010) Halofuginone inhibits Smad3 phosphorylation via the PI3K/Akt and MAPK/ERK pathways in muscle cells: effect on myotube fusion. *Exp. Cell Res.* **316**, 1061–1069
37. Zhang, Y. E. (2018) Mechanistic insight into contextual TGF- $\beta$  signaling. *Curr. Opin. Cell Biol.* **51**, 1–7
38. Tang, L. Y., Heller, M., Meng, Z., Yu, L. R., Tang, Y., Zhou, M., and Zhang, Y. E. (2017) Transforming growth factor- $\beta$  (TGF- $\beta$ ) directly activates the JAK1-STAT3 axis to induce hepatic fibrosis in coordination with the SMAD pathway. *J. Biol. Chem.* **292**, 4302–4312

Received for publication June 30, 2018.  
Accepted for publication November 19, 2018.